PCCP

PAPER

View Article Online
View Journal | View Issue

Cite this: *Phys. Chem. Chem. Phys.*, 2021, **23**, 10536

Noncovalent bond between tetrel π-hole and hydride†

Na Liu,[a] Jiaxing Liu,[a] Qingzhong Li *[a] and Steve Scheiner *[b]

Received 21st March 2021,
Accepted 20th April 2021

DOI: 10.1039/d1cp01245b

rsc.li/pccp

The π-hole above the plane of the $X_2T'Y$ molecule (T′ = Si, Ge, Sn; X = F, Cl, H; Y = O, S) was allowed to interact with the TH hydride of $TH(CH_3)_3$ (T = Si, Ge, Sn). The resulting TH···T′ tetrel bond is quite strong, with interaction energies exceeding 30 kcal mol^{-1}. $F_2T'O$ engages in the strongest such bonds, as compared to $F_2T'S$, $Cl_2T'O$, or $Cl_2T'S$. The bond weakens as T′ grows larger as in Si > Ge > Sn, despite the opposite trend in the depth of the π-hole. The reverse pattern of stronger tetrel bond with larger T is observed for the Lewis base $TH(CH_3)_3$, even though the minimum in the electrostatic potential around the H is nearly independent of T. The TH···T′ arrangement is nonlinear which can be understood on the basis of the positions of the extrema in the molecular electrostatic potentials of the monomers. The tetrel bond is weakened when H_2O forms an O···T′ tetrel bond with the second π-hole of $F_2T'O$, and strengthened if H_2O participates in an OH···O H-bond.

1. Introduction

Recent years have witnessed rapidly accelerating attention toward a type of noncovalent bond between an atom of Group 14 and an electron donor.[1] This tetrel bond (TB) plays an important role in crystal materials,[2–4] chemical reactions,[5–7] molecular recognition,[8–10] and biological systems,[11–13] just as do hydrogen and halogen bonds. As just one example as to how tetrel bonds can be incorporated into chemical thinking, the proton affinity on the oxygen atom in silanol and siloxane derivatives can be enhanced by the formation of a TB between the Si atom and several small Lewis bases.[14]

A simple means of understanding the origin of the tetrel bond may be derived from analysis of the molecular electrostatic potential (MEP) of the individual monomers. An area of positive MEP occurs on the tetrel atom surface, which facilitates its binding to an electron donor.[1] In the case of a sp^3-hybridized T atom, a positive region of this sort, termed a σ-hole, appears directly opposite each of the four covalent bonds in which the T atom participates. In the alternate case of sp^2 hybridization, the positive region is called a π-hole and lies above the plane of the molecule. Another aspect of TB stabilization arises from orbital interactions. For the σ-hole tetrel bond, there is a certain amount of charge transfer from the electron donor orbital, typically a lone pair, into the σ*(T–R) antibonding orbital (T = tetrel, and R its substituent). In addition to stabilizing the intermolecular tetrel bond, this transfer also weakens and lengthens the T–R covalent bond.[15]

The strength of a TB can be modulated through variation of substituents[16–27] and by cooperativity.[28–39] Generally, electron-withdrawing groups on the tetrel-containing Lewis acid intensify the σ-hole and thus strengthen the TB. Likewise, electron-donating groups on the nucleophile facilitate the transfer to the acid, and similarly enhance the bond. As specific examples, a systematic study of F-substitution[16] showed the TB in $TH_4\cdots NH_3$ (T = Si, Ge, Sn) is strengthened when the H opposite NH_3 is replaced by the electron-withdrawing F.[16] Strengthening also arises when the three peripheral H atoms of TH_4 are replaced by F.[16] These two sorts of fluorination patterns can cooperatively enhance the TB.[16] As another example, CH_3F forms only a weak TB with the π-system of C_2H_2 (1.2 kcal mol^{-1}), but the interaction is intensified fivefold when the two H atoms of acetylene are replaced by Na.[17] The coinage metal of MCN (M = Cu, Ag, Au) also has an enhancing effect on the TB in $MCN\cdots TF_4$, and its enhancing effect is dependent on the nature of both the coinage metal and T atoms, growing in the M = Au < Cu < Ag and T = C < Si < Ge < Sn orders.[18] For example, the interaction energy increases fourfold from $HCN\cdots SiF_4$ to $AgCN\cdots SiF_4$.[18] Formamidine can form a strong TB with SiH_3F (14.5 kcal mol^{-1}) and adding a methyl group to formamidine further increases the interaction energy to 19 kcal mol^{-1}.[19]

Like many of its cousins, TBs are also subject to cooperativity in that other noncovalent bonds within the system can strengthen

[a] *The Laboratory of Theoretical and Computational Chemistry, School of Chemistry and Chemical Engineering, Yantai University, Yantai 264005, People's Republic of China. E-mail: liqingzhong1990@sina.com; Fax: +86 535 6902063; Tel: +86 535 6902063*

[b] *Department of Chemistry and Biochemistry, Utah State University, Logan, UT 84322-0300, USA. E-mail: steve.scheiner@usu.edu*

† Electronic supplementary information (ESI) available: Tables S1–S5. See DOI: 10.1039/d1cp01245b

or weaken the TB.[28–39] As an example, when the π-hole on the carbon atom and the σ-hole on the chalcogen atom in F_2CSe and F_2CTe simultaneously bind with an electron donor, both the tetrel bond and the chalcogen bond are weakened, showing anticooperativity.[28] If a second HCN molecule forms a hydrogen bond with the first HCN molecule in $F_2TO\cdots HCN$ (T = C and Si), the tetrel bond is strengthened.[35] TF_3OH (T = C, Si, Ge) can bind with three nitrogen-containing bases HCN, NH_3, and imidazole through a hydrogen bond or a tetrel bond, and the hydrogen bond is preferred over the tetrel bond for most systems, excluding complexes of GeF_3OH with either NH_3 or imidazole.[39] $MgCl_2$ engages in a magnesium bond with the oxygen atom of TF_3OH, and it generally reinforces and accentuates the preference for the hydrogen bond or tetrel bond that is already present in the dimer.[39]

Various sorts of electron donors participate in TBs, ranging from lone pairs, anions, and π-electron systems, to metal hydrides, radicals, and carbenes.[15,40–45] In the case of metal hydrides, the corresponding interaction has been termed a tetrel-hydride TB,[15,42] which has undergone only minimal study. As another issue, the TBs which are stabilized through a π-hole are less well characterized than their σ-hole counterparts. With respect to cooperativity and its influence on π-hole TBs, it was found that when F_2SiO interacts with the hydroxyl oxygen of malondialdehyde, its intramolecular $OH\cdots O$ hydrogen bond is strengthened and a proton transfer occurs.[46] However, a similar proton transfer takes place in glycine when F_2SiO attacks its carbonyl oxygen atom.[47]

The current work attempts to fill in some of the gaps in our current understanding of these unusual sorts of noncovalent bonds. As π-hole donor, a series of planar $X_2T=Y$ molecules are considered. The central T atom includes the full set Si, Ge, and Sn. Both O and S are considered as the Y chalcogen atom which engages in a double bond to T. Halogen atoms X = F and Cl are both added, as well as H as a reference point. The H atom of $TH(CH_3)_3$ will bear a partial negative charge so will be attracted to the central T atom of $X_2T=Y$ so as to form a $TH\cdots T$ tetrel hydride bond. (Note that this arrangement is quite distinct from any sort of H-bond where the bridging H is positively polarized.) With neither a lone pair nor π-system available, the $TH(CH_3)_3$ electron donor will be unable to engage in a conventional tetrel bond, so will be forced to use alternate orbitals as its electron source. In order to cover a wide scope of such interactions Si, Ge, and Sn are all used as the central T atom of $TH(CH_3)_3$.

The calculations described below are intended to probe several questions. First, can a $TH\cdots T$ tetrel hydride bond be formed between these species, and how strong might such a bond be? Will such a bond be a linear one as is typical of both TBs and HBs, or does its unusual composition lead to non-linear arrangements? How is the strength of this sort of interaction affected by the nature of the two T atoms and the substituents on the $X_2T=Y$ acid? Which particular orbitals will be active in the charge transfers between the two monomers? With respect to cooperativity, how will the tetrel hydride bond be affected by the addition of a third molecule, and to which specific site will this added molecule be attracted?

2. Theoretical methods

The MP2/aug-cc-pVTZ protocol was used to optimize the structures of each complex and its constituent monomers. For the Sn atom, the aug-cc-pVTZ-PP basis set including a relativistic pseudopotential was used to account for relativistic effects.[48] Frequency calculations at the same level ensure these structures to be true minima. The interaction energy was defined as the difference between the energy of the complex and the energy sum of the monomers, with their geometry taken from the complex. Using the counterpoise method of Boys and Bernardi,[49] this quantity was corrected for the basis set superposition error (BSSE). All calculations were performed using Gaussian 09 software.[50]

The wave function analysis-surface analysis suite (WFA-SAS) program[51] was used to analyze the molecular electrostatic potential (MEP) of monomers and complexes on the 0.001 e $bohr^{-3}$ isosurface. Using AIM2000 software,[52] atoms in molecules (AIM) analysis was performed to obtain topological parameters of each bond critical point (BCP), including electron density (ρ), its Laplacian ($\nabla^2\rho$) and total energy density (H). The natural bond orbital (NBO) procedure performed by the NBO5.0 program[53] provided information concerning charge transfer and its energetic consequences. Multiwfn and VMD[54,55] were utilized to map noncovalent interactions (NCI). To probe the origin of stabilization, the GAMESS program[56] was used to carry out a local molecular orbital-energy decomposition analysis (LMOEDA)[57] decomposition of the interaction energy at the MP2/aug-cc-pVTZ(PP) level.

3. Results

3.1 Monomers

Since one can anticipate that the positive region of the Lewis acid will attract the negative region on the base, a preliminary analysis involves a description of the molecular electrostatic potential (MEP) that surrounds each monomer. As may be seen in Fig. 1a, each X_2TY molecule contains a positive region directly above (and below) the molecular plane, lying near the T atom, but shifted a bit toward the two X atoms. This area is typically designated as a π-hole, and the value of its MEP is quantified as the maximum value of the MEP, on the 0.001 au

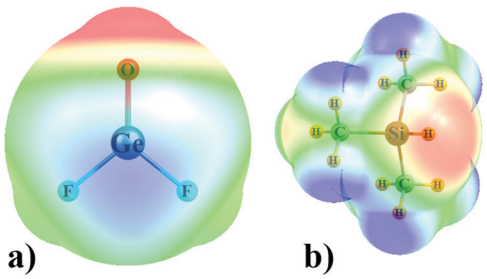

Fig. 1 MEP maps of sample Lewis acid and base monomers on a surface corresponding to 1.5× vdW radii. Red and blue indicate most negative and positive regions, respectively. The extrema are ±37 kcal mol^{-1} for F_2GeO and ±9 kcal mol^{-1} for $(CH_3)_3SiH$.

Table 1 The most positive MEP (V_{max}, kcal mol^{-1}) on the π-hole of $X_2T'Y$, and the most negative MEP (V_{min}, kcal mol^{-1}) on the H atom of T–H bond in $TH(CH_3)_3$, along with the angles (θ, deg.) describing their placement within each monomer

	V_{max}	θ(YT′···max)		V_{min}	θ(TH···min)
F_2SiO	80.82	105.5	$SiH(CH_3)_3$	−8.53	152.6
F_2GeO	77.50	107.3	$GeH(CH_3)_3$	−8.72	153.9
F_2SnO	85.72	105.5	$SnH(CH_3)_3$	−8.97	155.0
F_2SiS	67.77	109.3			
F_2GeS	66.77	110.4			
F_2SnS	77.12	110.7			
Cl_2SiO	55.97	99.7			
Cl_2GeO	56.35	101.4			
Cl_2SnO	68.21	112.1			
Cl_2SiS	46.06	103.7			
Cl_2GeS	48.07	105.9			
Cl_2SnS	61.81	102.6			

isodensity surface. The measure of this π-hole is displayed in Table 1 as V_{max} and follows certain patterns. It is larger for the more highly electron-withdrawing F substituents in F_2TY as compared to Cl_2TY. The same yardstick applies to the more electronegative O as compared to S, so X_2TO has a deeper π-hole than does X_2TS. And finally, there is an increasing trend with regard to the central T atom: Si ∼ Ge < Sn. $TH(CH_3)_3$ contains a minimum in its MEP near the TH hydrogen atom, as indicated by the red region in Fig. 1b. As may be seen in Table 1, there is little dependence of the depth of this minimum upon the nature of the central tetrel atom, all roughly equal to −8.78 kcal mol^{-1}.

Also listed in Table 1 are the positions of these extrema. The maximum in the MEP does not lie directly above the central T′ atom of $X_2T'Y$, as the θ(YT′···max) angles are all larger than 90°, which would place this point closer to the two X atoms. With respect to the location of the MEP minima in $TH(CH_3)_3$, these points lie off of the TH axis by some 15°–17°. The relevance of these positions will become clear below.

3.2 Dimers

3.2.1 Geometries and energetics. The general structure of each heterodimer is pictured in Fig. 2 where the H atom of $TH(CH_3)_3$ acts as a bridge between the two T atoms. The distance

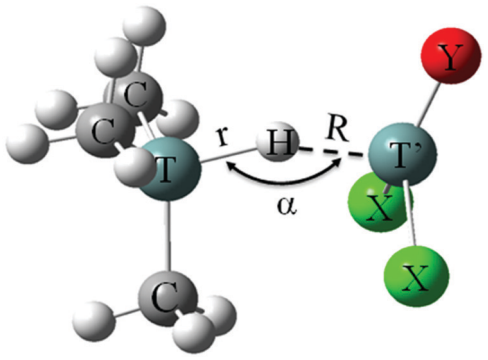

Fig. 2 Geometrical parameters defined for $(CH_3)_3TH\cdots T'X_2Y$ binary complexes.

Table 2 Interaction energy of dimers, E^{int} (kcal mol^{-1})

	E^{int}		E^{int}
$SiH(CH_3)_3\cdots F_2SiO$(**B1**)	−23.59	$SiH(CH_3)_3\cdots Cl_2SiO$(**B19**)	−17.49
$SiH(CH_3)_3\cdots F_2GeO$(**B2**)	−21.02	$SiH(CH_3)_3\cdots Cl_2GeO$(**B20**)	−15.37
$SiH(CH_3)_3\cdots F_2SnO$(**B3**)	−19.98	$SiH(CH_3)_3\cdots Cl_2SnO$(**B21**)	−15.78
$GeH(CH_3)_3\cdots F_2SiO$(**B4**)	−24.76	$GeH(CH_3)_3\cdots Cl_2SiO$(**B22**)	−20.96
$GeH(CH_3)_3\cdots F_2GeO$(**B5**)	−22.53	$GeH(CH_3)_3\cdots Cl_2GeO$(**B23**)	−16.73
$GeH(CH_3)_3\cdots F_2SnO$(**B6**)	−21.21	$GeH(CH_3)_3\cdots Cl_2SnO$(**B24**)	−16.84
$SnH(CH_3)_3\cdots F_2SiO$(**B7**)	−31.51	Sn $H(CH_3)_3\cdots Cl_2SiO$(**B25**)	−27.96
$SnH(CH_3)_3\cdots F_2GeO$(**B8**)	−30.10	$SnH(CH_3)_3\cdots Cl_2GeO$(**B26**)	−23.24
$SnH(CH_3)_3\cdots F_2SnO$(**B9**)	−28.40	$SnH(CH_3)_3\cdots Cl_2SnO$(**B27**)	−22.45
$SiH(CH_3)_3\cdots F_2SiS$(**B10**)	−22.69	$SiH(CH_3)_3\cdots Cl_2SiS$(**B28**)	−20.22
$SiH(CH_3)_3\cdots F_2GeS$(**B11**)	−19.08	$SiH(CH_3)_3\cdots Cl_2GeS$(**B29**)	−14.51
$SiH(CH_3)_3\cdots F_2SnS$(**B12**)	−19.00	$SiH(CH_3)_3\cdots Cl_2SnS$(**B30**)	−15.42
$GeH(CH_3)_3\cdots F_2SiS$(**B13**)	−22.31	$GeH(CH_3)_3\cdots Cl_2SiS$(**B31**)	−19.60
$GeH(CH_3)_3\cdots F_2GeS$(**B14**)	−20.54	$GeH(CH_3)_3\cdots Cl_2GeS$(**B32**)	−15.96
$GeH(CH_3)_3\cdots F_2SnS$(**B15**)	−20.18	$GeH(CH_3)_3\cdots Cl_2SnS$(**B33**)	−16.55
$SnH(CH_3)_3\cdots F_2SiS$(**B16**)	−28.89	$SnH(CH_3)_3\cdots Cl_2SiS$(**B34**)	−26.40
$SnH(CH_3)_3\cdots F_2GeS$(**B17**)	−27.83	$SnH(CH_3)_3\cdots Cl_2GeS$(**B35**)	−22.44
$SnH(CH_3)_3\cdots F_2SnS$(**B18**)	−27.09	$SnH(CH_3)_3\cdots Cl_2SnS$(**B36**)	−22.16

of H away from the T of $TH(CH_3)_3$ to which it is covalently attached is defined as r, while R refers to its distance from the T atom of the acid (designated as T′). The arrangement is not purely linear, as the α(TH···T′) angle differs from 180°. The interaction energies for each heterodimer, combining a $X_2T'Y$ with a $TH(CH_3)_3$ base, are reported in Table 2, and the salient geometrical parameters are displayed in Table 3. Due to the negative polarization of the H atom, and its direct interaction with T′, these complexes are characterized as hydride-tetrel bonds.

The interaction energies fall in the general range between 14.5 and 31.5 kcal mol^{-1}, so these interactions are rather strong as a group. There are a number of overarching trends that characterize these systems. The noncovalent bond energies diminish along with the size of the T′ atom in the acid in the order Si > Ge > Sn. Note that this trend runs counter to the deepening π-hole as the T′ atom enlarges, as documented in Table 1. However, this order reverses in the base as E^{int} rises along with the size of the T atom, with a particularly large jump from Ge to Sn. This trend is distinct from what may have been predicted based on V_{min} which is essentially independent of T. With regard to substituents, the fluorosubstituted $F_2T'Y$ acids engage in stronger interactions than their $Cl_2T'Y$ counterparts, by some 3–7 kcal mol^{-1}. And finally, the replacement of the O atom of $X_2T'O$ by S yields a modest decline. The latter two trends match the patterns observed in V_{max} and V_{min} in Table 1.

As is evident in Table 3, the intermolecular distance R elongates as T′ grows in size, caused by its increasing tetrel atomic radius. With respect to the T atom of the base, larger atoms have a contracting effect on the distance, consonant with the growing interaction energy. The replacement of F atoms on the acid by Cl results in a longer intermolecular separation, consistent with the weakened interaction. Also obeying the energetic trends, the swapping out of the O atom by S induces a slight bond stretch in most cases, with some exceptions.

The next column of Table 3 contains the stretch of the T–H covalent bond caused by the dimerization. These stretches are fairly large, as much as 0.13 Å, and they do not conform to the

Table 3 T–H···T′ distance (R, Å), change of T–H bond length (Δr, Å), and angles (θ, deg.) in the binary systems

	R	Δr	α(TH···T′)	θ(YT′···H)		R	Δr	α(TH···T′)	θ(YT′···H)
B1	1.693	0.071	139.3	104.0	**B19**	1.708	0.062	151.6	103.4
B2	1.741	0.075	139.9	107.1	**B20**	1.786	0.058	151.2	103.8
B3	1.944	0.068	139.7	109.0	**B21**	1.958	0.053	151.9	104.7
B4	1.684	0.079	137.7	104.1	**B22**	1.693	0.059	150.3	103.9
B5	1.729	0.085	138.1	107.7	**B23**	1.766	0.056	149.8	104.5
B6	1.937	0.077	137.9	109.8	**B24**	1.949	0.051	149.6	105.3
B7	1.645	0.112	134.9	106.6	**B25**	1.644	0.102	145.9	106.4
B8	1.686	0.132	134.1	111.0	**B26**	1.711	0.101	146.2	107.5
B9	1.901	0.125	133.1	114.4	**B27**	1.915	0.096	145.3	108.1
B10	1.710	0.072	134.9	111.2	**B28**	1.711	0.073	137.2	111.2
B11	1.752	0.073	140.2	108.9	**B29**	1.785	0.059	152.1	106.1
B12	1.943	0.066	139.9	111.2	**B30**	1.938	0.052	153.5	107.3
B13	1.694	0.079	138.1	105.9	**B31**	1.691	0.060	151.1	105.7
B14	1.738	0.082	138.4	109.2	**B32**	1.764	0.056	150.7	106.6
B15	1.936	0.075	138.3	111.7	**B33**	1.938	0.051	151.1	107.7
B16	1.652	0.113	134.9	108.0	**B34**	1.642	0.106	145.4	107.6
B17	1.692	0.127	134.2	112.1	**B35**	1.707	0.105	146.1	109.0
B18	1.899	0.122	133.3	115.6	**B36**	1.905	0.097	145.9	110.2

interaction energy patterns in Table 2. For example, these stretches tend to be largest for F_2GeO as compared to the Si and Sn analogues, even though this acid does not have the strongest interaction energy.

The nonlinearity of the TH···T′ arrangement is quantified by the α angles which lie in the general range of 133°–152°. These angles are closer to linearity for the Cl-substituted Lewis acids, but show few patterns with respect to other aspects of the dimers, such as the nature of T or T′, or O *vs.* S. The nonlinearity of the tetrel bond can be ascribed in large part to electrostatic considerations. As mentioned earlier, the σ-hole maximum of $X_2T'Y$ does not lie directly above the T′ atom but is shifted toward the two X atoms. This property helps explain the bending of the complex, as the θ(YT′···H) angles are fairly similar to the θ(YT′···max) angles within the monomers. For example, the latter angle situates the V_{max} of F_2SiO 105.5° from the perpendicular, which compares nicely with θ(YT′···H) angles of 104.0°, 104.1°, and 106.6° when F_2SiO is paired respectively with the Si, Ge, and Sn versions of $TH(CH_3)_3$. Another factor contributing to the bending of each complex arises from the locations of the V_{min} points of $TH(CH_3)_3$, lying some 153°–155° from the T–H axis (see Table 1). And indeed, many of the α angles in Table 3 lie close to this range.

3.2.2 Analysis of wave functions. In addition to the interaction energies, another measure of the strength of these tetrel-hydride bonds arises through AIM analysis of the electron density topology. The values of the density and its Laplacian at the H···T′ bond critical point are contained in Table 4, along with the total energy density H. Categorization of these interactions as strong noncovalent bonds is verified by the values of ρ which can be as high as 0.085 a.u., and by the fairly large positive density Laplacians. On the other hand, the negative values of H, although of small magnitude, might suggest partial covalent character to these bonds. The values of ρ are consistently maximized for X_2GeY, regardless of the nature of X and Y, which does not fit into the pattern of E^{int}, where it is T′ = Si that is largest. Nor is there agreement in terms of the comparison between $X_2T'O$ *vs.* $X_2T'S$ wherein ρ_{BCP} shows little distinction. Thus the electron density found at tetrel BCPs does not correlate with the interaction energy.

Table 4 Electron density (ρ), Laplacian ($\nabla^2\rho$), and total energy density (H) at the H···T′ BCP in the binary systems, all in a.u.

	ρ	$\nabla^2\rho$	H		ρ	$\nabla^2\rho$	H
B1	0.0608	0.1004	−0.0278	**B19**	0.0598	0.0779	−0.0280
B2	0.0728	0.0862	−0.0303	**B20**	0.0657	0.0731	−0.0247
B3	0.0574	0.1162	−0.0159	**B21**	0.0552	0.1071	−0.0152
B4	0.0608	0.1371	−0.0246	**B22**	0.0627	0.0837	−0.0299
B5	0.0759	0.0831	−0.0326	**B23**	0.0694	0.0715	−0.0275
B6	0.0590	0.1153	−0.0167	**B24**	0.0569	0.1071	−0.0161
B7	0.0711	0.1290	−0.0348	**B25**	0.0718	0.1172	−0.0356
B8	0.0862	0.0861	−0.0408	**B26**	0.0809	0.0775	−0.0363
B9	0.0657	0.1281	−0.0197	**B27**	0.0629	0.1191	−0.0187
B10	0.0582	0.1193	−0.0238	**B28**	0.0593	0.1112	−0.0247
B11	0.0713	0.0830	−0.0291	**B29**	0.0660	0.0729	−0.0249
B12	0.0575	0.1161	−0.0160	**B30**	0.0565	0.1101	−0.0160
B13	0.0634	0.0876	−0.0308	**B31**	0.0615	0.1171	−0.0261
B14	0.0747	0.0808	−0.0316	**B32**	0.0701	0.0720	−0.0280
B15	0.0591	0.1161	−0.0168	**B33**	0.0580	0.1101	−0.0167
B16	0.0717	0.1142	−0.0361	**B34**	0.0735	0.1110	−0.0374
B17	0.0854	0.0844	−0.0401	**B35**	0.0819	0.0775	−0.0371
B18	0.0660	0.1291	−0.0198	**B36**	0.0643	0.1221	−0.0194

As in H-bonds and other noncovalent bonds such as tetrel bonds, the complexes are stabilized in part by charge transfer. The total charge transferred from the Lewis base molecule to the acid are denoted as CT, which may be seen in Table 5 to fall into the range between 0.1 and 0.3 *e*. The replacement of the O atom of X_2TO to S tends to enlarge this charge transfer which is consistent with the more polarizable nature of S. There is similar, albeit smaller, effect arising from replacing the F substituents by Cl. Among the various T′ atoms, it is Ge that causes the largest transfer, similar to the pattern for ρ_{BCP}. There is greater sensitivity to the identity of the T atom in $TH(CH_3)_3$, where CT rises quickly along with atom size Si < Ge < Sn.

As a refinement of the total intermolecular charge transfer, NBO offers a means of considering transfers between individual

Table 5 Total charge transferred between molecules (CT, *e*) and second-order perturbation energies ($E^{(2)}$, kcal mol^{-1}) for transfer from σ(TH) orbital into indicated antibonding orbitals

	CT	$LP^*_{T'}$	$\sigma^*_{T'-X}$	$\sigma^*_{T'-Y}$		CT	$LP^*_{T'}$	$\sigma^*_{T'-X}$	$\sigma^*_{T'-Y}$
B1	0.156	85.93	16.27	2.25	**B19**	0.172	94.82	14.46	3.38
B2	0.162	81.29	19.47	2.75	**B20**	0.157	82.03	13.77	3.81
B3	0.105	59.69	—	10.05	**B21**	0.113	57.88	14.11	5.30
B4	0.179	96.31	17.12	2.32	**B22**	0.199	107.06	15.35	3.31
B5	0.188	91.03	20.77	2.84	**B23**	0.184	92.77	14.96	3.85
B6	0.124	67.95	—	10.45	**B24**	0.133	64.20	15.17	5.38
B7	0.224	—	—	—	**B25**	0.261	—	—	—
B8	0.240	—	—	—	**B26**	0.243	131.63	20.08	3.93
B9	0.165	95.62	—	13.64	**B27**	0.172	85.52	20.03	7.01
B10	0.175	—	25.74	69.99	**B28**	0.207	121.74	17.61	3.05
B11	0.171	87.97	24.96	1.51	**B29**	0.173	—	21.58	66.00
B12	0.121	65.49	—	7.50	**B30**	0.128	66.13	19.35	3.34
B13	0.195	—	—	—	**B31**	0.215	119.36	19.69	2.15
B14	0.201	—	—	—	**B32**	0.202	103.02	18.61	2.00
B15	0.141	82.18	—	7.62	**B33**	0.156	72.54	19.32	3.71
B16	0.248	—	—	—	**B34**	0.279	—	—	—
B17	0.266	—	—	—	**B35**	0.275	—	—	—
B18	0.186	113.50	—	9.28	**B36**	0.193	98.01	27.09	4.05

molecular orbitals. The bulk of the transfers arise from the σ(TH) bonding orbital of the Lewis base, but there are three orbitals of the acid to which this charge is shifted. There is first the unoccupied lone pair-type orbital of the T′ atom, primarily constituted of a p_π orbital. Other recipients are the σ*(T′Y) and σ*(T′X) orbitals. The second-order perturbation energies $E^{(2)}$ associated with each of these transfers are listed in Table 5. The largest contributor, with $E^{(2)}$ approaching and exceeding 100 kcal mol^{-1} is the transfer into the former LP* orbital. The pair of antibonding T′–X orbitals account for a fairly large contribution as well, and when these are absent, the σ*(T′Y) orbitals make up the difference. (It might be noted that there are several cases where the NBO treatment views the complex as a single entity, so there are no $E^{(2)}$ entries, as for example in B7 and B8.) There is a trend of diminishing $E^{(2)}$ values as T′ or T are enlarged, although there is little distinction between F and Cl on the $X_2T'Y$ monomer. The covalent character of the T–H bond is confirmed by the small electronegativity difference between T and H elements and the negative energy density at the T–H BCP (Table S1, ESI†).[58]

Another perspective on the nature of these noncovalent bonds is derived from a partitioning of the total interaction energy into various physically meaningful contributions. The values of the electrostatic, exchange, repulsion, polarization, and dispersion components are listed in Table S2 (ESI†) for each of the binary complexes. It may be stressed that the polarization term encompasses both intramolecular and intermolecular shifts of density, the latter of which is commonly referred to as charge transfer. There is a clear ordering of these contributions in that the exchange term is largest, followed by polarization which is in turn slightly larger than electrostatics, with dispersion making the smallest contribution. There is a fairly consistent quantitative pattern in that the polarization component accounts for some 47–57% of the total of (ES + POL + DISP), whereas ES makes up 39–49% of this total, and the dispersion is much smaller, less than 10%. Dispersion makes its largest contributions for larger atoms, *e.g.* $Cl_2T'S$ *vs.* $F_2T'O$. The electrostatic component does not necessarily follow the same trends as do the π-hole depths listed in Table 1.

As indicated above, the formation of each of these hydride tetrel bonds causes a substantial stretching of the internal *r*(TH) covalent bond. This stretch is associated with a red shift of the ν(TH) stretching frequency, which is displayed in Table S3 (ESI†). These frequency changes are rather substantial, ranging between 57 and 134 cm^{-1}. Unlike the stretches themselves, the red shifts are largest for the lighter T atoms. Also reported in Table S3 (ESI†) are the stretches of the T′═Y bonds within the Lewis acid unit. Although smaller than Δ*r*(TH), these elongations are appreciable as well, as much as 0.025 Å. The S atom stretches further from T′ by more than does O. Even though Δ*r*(T′Y) is smaller than is Δ*r*(TH), the red shifts of the latter bond are generally of larger magnitude, with a range of 71–285 cm^{-1}, so might serve as a particularly useful diagnostic tool. Raghavendra and Arunan thought that big shifts are sometimes caused by the mixing of modes between donor and acceptor,[59] however, it is only true for the T–H stretch vibration in $SiH(CH_3)_3\cdots H_2SnO$, $SiH(CH_3)_3\cdots H_2SnS$ and $SnH(CH_3)_3\cdots F_2CO$ and it is local vibrations in most systems.

3.3 Triads

After the $TH(CH_3)_3$ has occupied one of the two π-holes lying above $F_2T'O$, there remains a second such π-hole directly below T′. This second positive region could attract another Lewis base, as for example the O atom of H_2O. The ensuing triad which is characterized by a pair of tetrel bonds (**TT**) is illustrated in Fig. 3a. As an alternative, there is a strong negative region associated with the O atom of $F_2T'O$, which would attract the positive H atoms of the water molecule. A geometry of this sort with both a tetrel and a H-bond (**TH**) is diagrammed in Fig. 3b. One would anticipate on general grounds that the **TT** triad would experience negative cooperativity since both tetrel bonds require the $F_2T'O$ to serve as a dual electron acceptor. The HB within the TH structure, on the other hand, places this molecule in the position of simultaneous electron donor and acceptor which should accordingly result in positive cooperativity.

As an example of how the addition of the water might affect the ability of the $F_2T'O$ to engage in a $TH\cdots T'$ tetrel bond, the first three rows of Table 6 show that placement of the water near one π-hole of $F_2T'O$ reduces the depth of the other π-hole and so its ability to attract the hydride entity. This drop in V_{max} lies in the range of 16–36%. Conversely, the electron density transfer from $F_2T'O$ to H_2O when the latter forms an $OH\cdots O$ HB acts to deepen the π-hole, albeit by not quite as much, on the order of 3–8%, as witness the last three rows of Table 6.

The negative cooperativity of the **TT** trimers is plainly in evidence in the first nine rows of Table 7 where the addition of the water molecule with its second tetrel bond causes a marked elongation of the $TH\cdots T'$ tetrel bond relative to the dimer. This stretch is quite substantial, reaching up to as much as 0.6 Å. In striking contrast, the positive cooperativity arising when the water molecule engages in an $OH\cdots O$ HB with $F_2T'O$ contracts the TB by some 0.04–0.05 Å. The interaction energy reported in

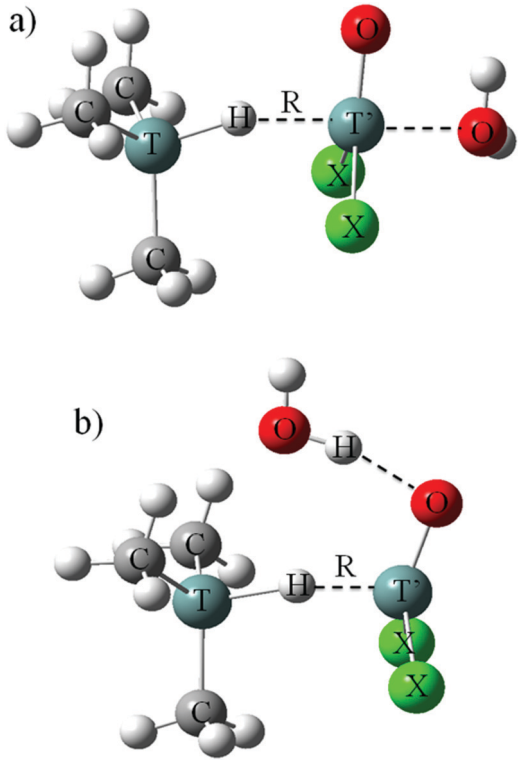

Fig. 3 Ternary complexes $TH(CH_3)_3\cdots X_2T'Y\cdots H_2O$ (a) TT, containing two tetrel bonds, and (b) TH, stabilized by one tetrel and one H-bond.

Table 6 The most positive MEP (V_{max}, kcal mol^{-1}) on the π-hole of T′ atom in the $F_2T'O\cdots H_2O$ complex and its change (ΔV_{max}, kcal mol^{-1}) relative to $F_2T'O$ monomer

	V_{max}	ΔV_{max}
$F_2SiO\cdots H_2O$(**A1**)	52.02	−28.80
$F_2GeO\cdots H_2O$(**A2**)	64.95	−12.55
$F_2SnO\cdots H_2O$(**A3**)	59.42	−26.29
$F_2SiO\cdots H_2O$(**A4**)	86.53	5.71
$F_2GeO\cdots H_2O$(**A5**)	83.58	6.09
$F_2SnO\cdots H_2O$(**A6**)	88.42	2.70

Table 7 refers to that between the $TH(CH_3)_3$ unit and either the $F_2T'O$ monomer or the $F_2T'O\cdots H_2O$ dimer in the case of the full triad. The deleterious effects of adding a second tetrel bond in the **TT** structures is clear in the positive entries in the last column of Table 7, which equate to a weakening of the $TH\cdots T'$ tetrel bond. This negative cooperativity is strongest for the smaller T′ atom Si and least dramatic for Sn. The cooperative effects of the HB and TB upon one another are likewise exemplified by the strengthening negative values for the TH triads in the last six rows. On a percentage basis, the negative cooperativity of the **TT** triads reduces the interaction energies to some 24–78% of their magnitude within the dimer. The largest reductions occur for the smaller T′ atoms. The **TH** positive cooperativity is manifested by magnifications of the interaction energy by up to 150%.

Fig. 4 displays the NCI diagram of the **TH** structure of $SiH(CH_3)_3\cdots F_2SiO\cdots H_2O$ as an illustrative example. The blue

Table 7 T–H···T′ distance (R, Å) and interaction energy of π-hole tetrel-hydride interaction (E_{int}, kcal mol^{-1}) in the ternary systems as well as their change (Δ) relative to the binary analogue

	R	ΔR	E_{int}	ΔE_{int}
$SiH(CH_3)_3\cdots F_2SiO\cdots H_2O$(**TT1**)	2.267	0.574	−5.70	17.89
$SiH(CH_3)_3\cdots F_2GeO\cdots H_2O$(**TT2**)	1.915	0.174	−11.01	10.01
$SiH(CH_3)_3\cdots F_2SnO\cdots H_2O$(**TT3**)	2.088	0.144	−13.53	6.45
$GeH(CH_3)_3\cdots F_2SiO\cdots H_2O$(**TT4**)	2.323	0.639	−7.47	17.29
$GeH(CH_3)_3\cdots F_2GeO\cdots H_2O$(**TT5**)	1.898	0.169	−11.57	10.96
$GeH(CH_3)_3\cdots F_2SnO\cdots H_2O$(**TT6**)	2.015	0.078	−13.91	7.30
$SnH(CH_3)_3\cdots F_2SiO\cdots H_2O$(**TT7**)	1.891	0.246	−8.03	23.48
$SnH(CH_3)_3\cdots F_2GeO\cdots H_2O$(**TT8**)	1.837	0.151	−14.81	15.29
$SnH(CH_3)_3\cdots F_2SnO\cdots H_2O$(**TT9**)	1.991	0.090	−22.14	6.26
$SiH(CH_3)_3\cdots F_2SiO\cdots H_2O$(**TH1**)	1.645	−0.048	−35.35	−11.76
$SiH(CH_3)_3\cdots F_2GeO\cdots H_2O$(**TH2**)	1.694	−0.047	−30.94	−9.92
$SiH(CH_3)_3\cdots F_2SnO\cdots H_2O$(**TH3**)	1.897	−0.047	−26.98	−7.00
$GeH(CH_3)_3\cdots F_2SiO\cdots H_2O$(**TH4**)	1.642	−0.042	−31.60	−6.84
$GeH(CH_3)_3\cdots F_2GeO\cdots H_2O$(**TH5**)	1.682	−0.047	−30.00	−7.47
$GeH(CH_3)_3\cdots F_2SnO\cdots H_2O$(**TH6**)	1.888	−0.049	−28.77	−7.56

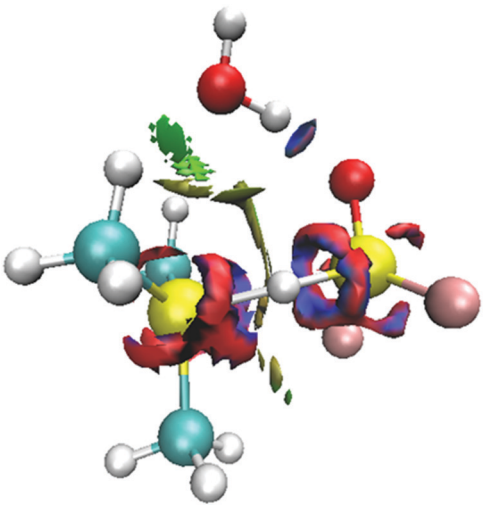

Fig. 4 NCI diagram of $SiH(CH_3)_3\cdots F_2SiO\cdots H_2O$ (**TH1**). Blue, red, and green regions denote strong attractive, strong repulsion, and weak attractive interactions, respectively.

disk between the H atom of H_2O and the O atom of F_2SiO, indicates the presence of a strong $OH\cdots O$ hydrogen bond. An irregular blue and red circle along the $H\cdots T'$ axis corresponds to a very strong tetrel bond. In addition, there is a green region between the O atom of H_2O and two H atoms of a methyl group, characteristic of a weak $C–H\cdots O$ hydrogen bond.

3.4 Unsubstituted dimers

It is finally of interest to examine how the results might change if the two electron-withdrawing X atoms of $X_2T'Y$ are replaced by H atoms. As indicated in Table S4 (ESI†), this change reduces the depth of the π-hole to only about 65% of its value in $X_2T'Y$. The interaction energies are likewise reduced to the amounts reported in Table S5 (ESI†). In fact, neither H_2SiO nor H_2GeO are able to form a stable complex with $SnH(CH_3)_3$. The weakening of the acid's π-hole results in a similar reduction in the interaction energies, which are only about 50–70% of the

corresponding values for the $F_2T'O$ acids. These same concepts apply as well to the stretch of the T–H bond induced by the complexation. The values of Δr for the unsubstituted acids in Table S5 (ESI†) are only 67–92% of what is observed for the fluorinated acids. The replacement of the X atoms of $X_2T'Y$ by H also results in a reduction of the stretch of the TH bond within $TH(CH_3)_3$, as evident in Table S6 (ESI†). In summary, the removal of the halogen atoms from the acid results in a fairly uniform reduction of all aspects of the interaction.

4. Discussion

There is a certain amount of deformation energy that occurs within the $F_2T'O$ molecule when it engages in a tetrel bond with $TH(CH_3)_3$, primarily the transition from planar to pyramidal structure. However, such deformation is reduced if the same T′ atom engages in two π-hole bonds with nucleophiles on both sides simultaneously. It is this diminished deformation which makes the tetrel bond strongest in the T′ = Si < Ge < Sn sequence within the $TH(CH_3)_3\cdots F_2T'O\cdots H_2O$(TT) triads, opposite to the pattern in the dimers where deformation plays a larger role.

A metal hydride unit can act as an electron donor to both the σ-hole or the π-hole[15] of a tetrel atom. HBeH and HMgH are commonly used as metal hydrides in studying non-covalent interactions. When either is added to F_2TO or TH_4, a reaction occurs rather than forming a tetrel-bonded complex. A future study of either an experimental or theoretical nature might be able to examine a tetrel-bonded entrance channel complex, parallel to what is seen in the F···H–F H-bonded structure.[60] Our use here of $TH(CH_3)_3$ as an electron donor avoids such a reaction by means of the steric hindrance introduced by the three methyl groups. For the σ-hole tetrel-hydride interaction in $HMH\cdots T'H_3F$ (M = Be and Mg; T′ = Si–Sn), the electrostatic contribution is larger than polarization.[15] However, an opposite result is found for the π-hole tetrel-hydride interaction. The main reason for this reversal is that larger distortion occurs for $X_2T'Y$ in the latter interaction. The smaller distortion of $T'H_3F$ is also reflected in its smaller charge transfer (<0.06 e).[15]

The π-hole on $X_2T'O$ also engages in a tetrel bond with other types of electron donors.[46,47,61–63] Similarly, these tetrel bonds involving $X_2T'O$ are also very strong, strong enough to cause a proton transfer in certain situations.[46,47]

In its common tetravalent bonding situation, as in TX_4, the tetrel atom is characterized by four σ-holes, opposite each of the four T–X bonds. Tetrel bonds to these σ-holes can be of variable strength, but climbing to more than 15 kcal mol^{-1} if amplified by a positive charge on the Lewis acid.[64] In an alternative trivalent molecular structure as in planar F_2TO, these positive regions are of π-hole type, lying above and below the plane. Another scenario which yields π-holes is linear molecules such as OCO. The latter can form a tetrel bond of perhaps 2–3 kcal mol^{-1},[65] likewise for XCN.[66] Indeed, the combination of OCO with HCN provides an early example[67] of what has come to be known as a tetrel bond.

There are indications that it is the latter π-hole which engages in stronger tetrel bonds in a general sense. For example, the interaction energy is −22.8 kcal mol^{-1} in $F_2OSi\cdots NCH$[35] but only −3.6 kcal mol^{-1} in $H_3FSi\cdots NCH$.[5] Interaction energies of σ-hole tetrel bonds with NH_3 as a base are quite variable, depending upon the substitution pattern, and nature of the tetrel atom. While TH_4 binds rather weakly, less than 3 kcal mol^{-1}, tetrafluorination to TF_4 raises this quantity up to as much as 25 kcal mol^{-1}.[16] Smaller changes accompany the replacement of the H atoms by alkyl groups.[68] The nature of the base is also a determining factor. For example, NCH binds much more weakly to TF_4 than does NH_3.[69]

Perhaps the most direct comparison of σ and π-hole tetrel bonds compared TH_4, TH_3F, and TH_2F_2 with the planar analogues $H_2T=CH_2$, HFT = CH_2, and $F_2T=CH_2$.[70] The σ-hole V_{max} varies from 20 to 60 kcal mol^{-1}, depending of course on degree of fluorosubstitution. The π-holes are just slightly shallower, in the 10–53 kcal mol^{-1} range. In terms of the tetrel bond energies, σ-hole bonds range between 1 and 20 kcal mol^{-1}, while the π-interaction energies are somewhat larger, between 4 and 29 kcal mol^{-1}. In the same vein but with a different sort of electron donor, TH_3F was compared with R_2TO, as σ and π-hole donors, respectively,[63] but using the π-electron system of an aromatic borazine unit as electron donor. In this scenario, it is the π-complexes that are more strongly bound.

There are several measures of charge transfer that have been elucidated. The CT quantity in Table 5 assesses the total amount of electron density that has been lost by the nucleophilic molecule and acquired by the acid unit. The $E^{(2)}$ quantities represent the energetic consequence of a transfer between individual localized NBO orbitals, one on the base and the other on the acid. These second-order perturbation energies are especially large for the transfer into the tetrel atom's p-orbital, indicative of a π-hole interaction. One aspect of the NBO treatment is that it does not separate the electrostatic contribution from the charge transfer energy.[71] The E^{pol} quantities in Table S2 (ESI†) arising from the energy decomposition analysis are also quite large, comparable to the electrostatic energy. However, it must be borne in mind that E^{pol} describes not only charge transfer but internal polarizations within each subunit. One might also note that the sum of the electrostatic and polarization energies is roughly comparable to the NBO interorbital transfer sums.

The issue changes a bit when a TF_4 molecule attempts to engage in two tetrel bonds simultaneously. In order to do so, the molecule must alter its shape in one of two ways.[72] A trigonal bipyramid contains two σ-holes, whereas there are two π-holes within a planar configuration. The latter has much larger interaction energies than does the former but the situation reverses when the deformation energy is added to the equation. So in summary, the answer to the question as to whether σ or π-hole tetrel bonds are favored is a complicated one.

One interesting facet of the systems considered here is the nonlinearity of the $TH\cdots T'$ arrangement. This finding is unexpected, particularly in light of the tendency toward linearity of both

H-bonds where the bridging H is positively polarized, and dihydrogen bonds where there is an opposite negative polarization on one of the H atoms. This nonlinearity was rationalized here by careful inspection of the disposition of the MEPs around each monomer. It will be interesting to see if these deviations from linearity are common to other interactions of this sort as well.

It is widely accepted that σ-holes result from electron density being drawn in toward a covalent bond, leaving a depletion along an extension of the bond. However, there is no clear consensus concerning the origin of π-holes. Kozuch[73] has shown that they can be attributed to various sources, including as an indirect result of several σ-holes, and has questioned whether several complexes in the literature are correctly attributed to π-hole bonds. The structures described herein may be labeled in this manner for several reasons. In the first place, the nucleophile is clearly drawn in toward the region above the acid's plane where a π-hole is clearly visible and is rather deep, on the order of 80 kcal mol^{-1}. There is a clear AIM bond path leading from the hydride H directly to the central tetrel atom, with a fairly large bond critical point density. NBO shows that the primary recipient of the charge being transferred to the Lewis acid is the tetrel atom's vacant p-orbital, with much less being directed to the σ* antibonding orbitals of the substituents.

Although AIM is widely used to identify atoms that are bonded to one another, the method is far from infallible. A number of situations have been described in the literature where AIM bond paths were misleading or misrepresented bond strengths.[74–81] NBO, too has several weaknesses, including the disagreements that have been noted when results are compared to those from ALMO.

5. Conclusions

The π-hole above the tetrel atom of planar $X_2T'Y$ is able to form a strong noncovalent bond with the negatively polarized H atom of $TH(CH_3)_3$. The geometry of the resulting complex contains a nonlinear TH···T′ arrangement due in part to the disposition of the MEP surrounding the two monomers. The fluorosubstituted $F_2T'Y$ engages in the strongest such bonds, with less sensitivity to $X_2T'S$ *vs.* $X_2T'O$. The bond weakens as T′ grows larger, despite the opposite trend in the depth of the π-hole. The reverse pattern of stronger TB with larger T is observed for the Lewis base $TH(CH_3)_3$, even though the minimum in the electrostatic potential surrounding the H is nearly independent of T. The engagement of the O atom of a water molecule with the second π-hole of $X_2T'Y$ weakens the tetrel hydride bond. In contrast, this bond is strengthened if the water forms an OH···Y H-bond with the Y atom of $X_2T'Y$.

Conflicts of interest

There are no conflicts to declare.

Acknowledgements

This work was supported by the National Natural Science Foundation of China (21573188) and by the US National Science Foundation (1954310).

References

1 A. Bauzá, T. J. Mooibroek and A. Frontera, *Angew. Chem., Int. Ed.*, 2013, **52**, 12317–12321.
2 M. S. Gargari, V. Stilinović, A. Bauzá, A. Frontera, P. McArdle, D. V. Derveer, S. W. Ng and G. Mahmoudi, *Chem. – Eur. J.*, 2015, **21**, 17951–17958.
3 A. Bauzá, S. K. Seth and A. Frontera, *Coord. Chem. Rev.*, 2019, **384**, 107–125.
4 S. Mirdya, S. Roy, S. Chatterjee, A. Bauzá, A. Frontera and S. Chattopadhyay, *Cryst. Growth Des.*, 2019, **19**, 5869–5881.
5 S. J. Grabowski, *Phys. Chem. Chem. Phys.*, 2014, **16**, 1824–1834.
6 A. Frontera and A. Bauzá, *Chem. – Eur. J.*, 2018, **24**, 16582–16587.
7 M. X. Liu, Q. Z. Li, J. B. Cheng, W. Z. Li and H. B. Li, *J. Chem. Phys.*, 2016, **145**, 224310.
8 S. Scheiner, *Molecules*, 2018, **23**, 1147.
9 S. Scheiner, *J. Phys. Chem. A*, 2017, **121**, 3606–3615.
10 A. Bauzá, R. Ramis and A. Frontera, *Comput. Theor. Chem.*, 2014, **1038**, 67–70.
11 X. García-LLinás, A. Bauzá, S. K. Seth and A. Frontera, *J. Phys. Chem. A*, 2017, **121**, 5371–5376.
12 Á. M. Montaña, *ChemistrySelect*, 2017, **2**, 9094–9112.
13 A. Bauzá and A. Frontera, *Crystals*, 2016, **6**, 26.
14 C. Martín-Fernández, M. M. Montero-Campillo, I. Alkorta and J. Elguero, *J. Phys. Chem. A*, 2017, **121**, 7424–7431.
15 Q. Z. Li, H. Y. Zhuo, H. B. Li, Z. B. Liu, W. Z. Li and J. B. Cheng, *J. Phys. Chem. A*, 2015, **119**, 2217–2224.
16 S. Scheiner, *J. Phys. Chem. A*, 2017, **121**, 5561–5568.
17 Y. X. Wei, H. B. Li, J. B. Cheng, W. Z. Li and Q. Z. Li, *Int. J. Quantum Chem.*, 2017, **117**, e25448.
18 Y. X. Wei, J. B. Cheng, W. Z. Li and Q. Z. Li, *RSC Adv.*, 2017, **7**, 46321–46328.
19 H. L. Xu, J. B. Cheng, X. F. Yu and Q. Z. Li, *ChemistrySelect*, 2018, **3**, 2842–2849.
20 M. C. Hou, S. B. Yang, Q. Z. Li, J. B. Cheng, H. B. Li and S. F. Liu, *Molecules*, 2019, **24**, 10.
21 W. B. Dong, X. Yang, J. B. Cheng, W. Z. Li and Q. Z. Li, *J. Fluorine Chem.*, 2018, **207**, 38–44.
22 Y. X. Wei, Q. Z. Li, X. Yang and S. A. C. McDowell, *ChemistrySelect*, 2017, **2**, 11104–11112.
23 M. D. Esrafili, H. Kiani and F. Mohammadian-Sabet, *Mol. Phys.*, 2016, **114**, 3658–3668.
24 W. B. Dong, Q. Z. Li and S. Scheiner, *Molecules*, 2018, **23**, 1681.
25 M. C. Hou, K. Y. Jin, Q. Z. Li and S. L. Liu, *RSC Adv.*, 2019, **9**, 18459–18466.
26 M. X. Liu, Q. Z. Li, W. Z. Li and J. B. Cheng, *J. Mol. Graphics Modell.*, 2016, **65**, 35–42.

27 J. E. Del Bene, I. Alkorta and J. Elguero, *Chem. Phys. Lett.*, 2019, **730**, 466–471.
28 X. Guo, Y. W. Liu, Q. Z. Li, W. Z. Li and J. B. Cheng, *Chem. Phys. Lett.*, 2015, **620**, 7–12.
29 M. Marín-Luna, I. Alkorta and J. Elguero, *J. Phys. Chem. A*, 2016, **120**, 648–656.
30 M. D. Esrafili, N. Mohammadirad and M. Solimannejad, *Chem. Phys. Lett.*, 2015, **628**, 16–20.
31 M. D. Esrafili and F. Mohammadian-Sabet, *Mol. Phys.*, 2016, **114**, 1528–1538.
32 M. Solimannejad, M. Orojloo and S. Amani, *J. Mol. Model.*, 2015, **21**, 183.
33 H. L. Xu, J. B. Cheng, X. Yang, Z. B. Liu, W. Z. Li and Q. Z. Li, *ChemPhysChem*, 2017, **18**, 2442–2450.
34 S. A. C. McDowell, *Chem. Phys. Lett.*, 2014, **598**, 1–4.
35 Q. J. Tang and Q. Z. Li, *Comput. Theor. Chem.*, 2014, **1050**, 51–57.
36 H. L. Xu, J. B. Cheng, X. Yang, Z. B. Liu, B. Xiao and Q. Z. Li, *RSC Adv.*, 2017, **7**, 21713–21720.
37 M. X. Liu, L. Yang, Q. Z. Li, W. Z. Li, J. B. Cheng, B. Xiao and X. F. Yu, *J. Mol. Model.*, 2016, **22**, 192.
38 I. Alkorta, M. M. Montero-Campillo, O. Mó, J. Elguero and M. Yáñez, *J. Phys. Chem. A*, 2019, **123**(32), 7124–7132.
39 M. C. Hou, Y. F. Zhu, Q. Z. Li and S. Scheiner, *ChemPhysChem*, 2020, **21**, 212–219.
40 J. E. Del Bene, I. Alkorta and J. Elguero, *Chem. Phys. Lett.*, 2016, **655–656**, 115–119.
41 D. Mani and E. Arunan, *J. Phys. Chem. A*, 2014, **118**, 10081–10089.
42 M. D. Esrafili and F. Mohammadian-Sabet, *J. Mol. Model.*, 2015, **21**, 206.
43 Q. Z. Li, X. Guo, X. Yang, W. Z. Li, J. B. Cheng and H. B. Li, *Phys. Chem. Chem. Phys.*, 2014, **16**, 11617–11625.
44 M. X. Liu, Q. Z. Li, W. Z. Li and J. B. Cheng, *Struct. Chem.*, 2017, **28**, 823–831.
45 J. E. Del Bene, I. Alkorta and J. Elguero, *J. Phys. Chem. A*, 2017, **121**, 4039–4047.
46 Y. X. Wei, Q. Z. Li and S. Scheiner, *ChemPhysChem*, 2018, **19**, 736–743.
47 M. C. Hou, Q. Z. Li and S. Scheiner, *Chem. Phys. Lett.*, 2019, **731**, 136584.
48 K. A. Peterson, D. Figgen, M. Dolg and H. Stoll, *J. Chem. Phys.*, 2007, **126**, 124101.
49 M. J. Frisch, G. W. Trucks, H. B. Schlegel, G. E. Scuseria, M. A. Robb, J. R. Cheeseman, G. Scalmani, V. Barone, B. Mennucci, G. A. Petersson, H. Nakatsuji, M. Caricato, X. Li, H. P. Hratchian, A. F. Izmaylov, J. Bloino, G. Zheng, J. L. Sonnenberg, M. Hada, M. Ehara, K. Toyota, R. Fukuda, J. Hasegawa, M. Ishida, T. Nakajima, Y. Honda,O. Kitao, H. Nakai, T. Vreven, J. J. A. Montgomery, J. E. Peralta, F. Ogliaro, M. Bearpark, J. J. Heyd, E. Brothers, K. N. Kudin, V. N. Staroverov, R. Kobayashi, J. Normand, K. Raghavachari, A. Rendell, J. C. Burant, S. S. Iyengar, J. Tomasi, M. Cossi, N. Rega, J. M. Millam, M. Klene, J. E. Knox, J. B. Cross, V. Bakken, C. Adamo, J. Jaramillo, R. Gomperts, R. E. Stratmann, O. Yazyev, A. J. Austin, R. Cammi, C. Pomelli, J. W. Ochterski, R. L. Martin, K. Morokuma, V. G. Zakrzewski, G. A. Voth, P. Salvador, J. J. Dannenberg, S. Dapprich, A. D. Daniels, O. Farkas, J. B. Foresman, J. V. Ortiz, J. Cioslowski and D. J. Fox, *Gaussian09, Revision A.02*, Gaussian Inc., Wallingford, CT, 2009.
50 S. F. Boys and F. Bernardi, *Mol. Phys.*, 1970, **19**, 553–558.
51 F. A. Bulat, A. Toro-Labbe, T. Brinck, J. S. Murray and P. Politzer, *J. Mol. Model.*, 2010, **16**, 1679–1691.
52 R. F. W. Bader, *AIM2000 Program, v. 2.0*, McMaster University, Hamilton, 2000.
53 A. E. Reed, L. A. Curtiss and F. Weinhold, *Chem. Rev.*, 1988, **88**, 899–926.
54 T. Lu and F. Chen, *J. Comput. Chem.*, 2012, **33**, 580–592.
55 W. Humphrey, A. Dalke and K. Schulten, *J. Mol. Graphics*, 1996, **14**, 33–38.
56 P. F. Su and H. Li, *J. Chem. Phys.*, 2009, **131**, 014102.
57 M. W. Schmidt, K. K. Baldridge, J. A. Boatz, S. T. Elbert, M. S. Gordon, J. H. Jensen, S. Koseki, N. Matsunaga, K. A. Nguyen, S. J. Su, T. L. Windus, M. Dupuis and J. A. Montgomery, *J. Comput. Chem.*, 1993, **14**, 1347–1363.
58 D. Cremer and E. Kraka, *Angew. Chem., Int. Ed. Engl.*, 1984, **23**, 627–628.
59 B. Raghavendra and E. Arunan, *J. Phys. Chem. A*, 2007, **111**, 9699–9706.
60 B. Dereka, Q. Yu, N. H. C. Lewis, W. B. Carpenter, J. M. Bowman and A. Tokmakoff, *Science*, 2021, **371**, 160–164.
61 M. C. Hou, Z. B. Liu and Q. Z. Li, *Int. J. Quantum Chem.*, 2020, **2010**, e26251.
62 W. B. Dong, B. B. Niu, S. F. Liu, J. B. Cheng, S. L. Liu and Q. Z. Li, *ChemPhysChem*, 2019, **20**, 627–635.
63 J. R. Zhang, Q. Z. Hu, Q. Z. Li and S. Scheiner, *Int. J. Quantum Chem.*, 2019, **119**, e25910.
64 S. Scheiner, *J. Phys. Chem. A*, 2015, **119**, 9189–9199.
65 L. M. Azofra and S. Scheiner, *J. Chem. Phys.*, 2015, **142**, 1719.
66 V. D. P. N. Nziko and S. Scheiner, *Phys. Chem. Chem. Phys.*, 2016, **18**, 3581–3590.
67 K. R. Leopold, G. T. Fraser and W. Klemperer, *J. Chem. Phys.*, 1984, **80**, 1039–1046.
68 S. Scheiner, *J. Phys. Chem. A*, 2018, **122**, 2550–2562.
69 W. Zierkiewicz, M. Michalczyk and S. Scheiner, *Phys. Chem. Chem. Phys.*, 2018, **20**, 8832–8841.
70 Z. Wiktor, M. Mariusz and S. Scheiner, *Molecules*, 2018, **23**, 1416–1437.
71 A. E. Reed, L. A. Curtiss and F. Weinhold, *Chem. Rev.*, 1988, **88**, 899–926.
72 M. Mariusz, W. Zierkiewicz, R. Wysokiński and S. Scheiner, *ChemPhysChem*, 2019, **20**, 959–966.
73 S. Kozuch, *Phys. Chem. Chem. Phys.*, 2016, **18**, 30366–30369.
74 R. Taylor, *CrystEngComm*, 2020, **22**, 7145–7151.
75 S. J. Grabowski, *Molecules*, 2020, **25**, 4668.
76 M. Jabłoński, *Chem. Phys. Lett.*, 2020, **759**, 137946.
77 M. Jabłoński, *ChemistryOpen*, 2019, **8**, 497–507.
78 D. Myburgh, *J. Comput. Chem.*, 2018, **39**, 2273–2282.
79 C. R. Wick and T. Clark, *J. Mol. Model.*, 2018, **24**, 142.
80 S. Shahbazian, *Chem. – Eur. J.*, 2018, **24**, 5401–5405.
81 Z. A. Keyvani, S. Shahbazian and M. Zahedi, *Chem. – Eur. J.*, 2016, **22**, 5003–5009.

